

Resolving phonon-mediated superconducting pairing symmetries from first-principles calculation

Zimeng Zeng,¹ Xiaoming Zhang,² Jian Wu,^{1,3} and Zheng Liu^{4,*}

¹*State Key Laboratory of Low Dimensional Quantum Physics,
Department of Physics, Tsinghua University, Beijing 100084, China*

²*College of Physics and Optoelectronic Engineering,
Ocean University of China, Qingdao, Shandong 266100, China*

³*Frontier Science Center for Quantum Information, Beijing, China.*

⁴*School of Physics, Beihang University, Beijing 100191, China*

(Dated: November 25, 2024)

The quest for topological superconductors triggers revived interests in resolving non- s -wave pairing channels mediated by phonons. While density functional theory and density functional perturbation theory have established a powerful framework to calculate electron-phonon couplings in real materials in a first-principles way, its application is largely limited to conventional s -wave superconductivity. Here, we formulate an efficient and simple-to-use algorithm for first-principles pairing channel analysis, and apply it to several representative material systems.

I. INTRODUCTION

In the past two decades, the first-principles calculation within the framework of density functional theory (DFT) has reached a status to reliably describe not only the normal states of a wide range of materials, but also conventional superconductivity (SC) mediated by phonons [1]. Calculating the electron-phonon couplings (EPCs) from first principle is rapidly reaching maturity, thanks to the development of density functional perturbation theory (DFPT) [2].

It is commonly known that the predominating pairing channel from phonons is of a s -wave symmetry, and the Cooper pairs form spin singlets. In practice, the spin degrees of freedom of EPCs are thus ignored in most first-principles calculations. To predict the superconducting transition temperature (T_c), the s -wave channel is implicitly assumed, either in McMillan-Allen-Dynes formula [3] or the self-consistent solution of Migdal-Eliashberg equations [4].

Recently, the potential role of phonons in achieving unconventional superconductivity attracts revived theoretical attentions. The concern is that while electron-electron Coulomb repulsion always suppresses the conventional s -wave pairing, it can be collaborative with phonons in stabilizing other pairing symmetries, e.g. in a topological superconductor [5–7], or in high- T_c cuprate and pnictides superconductors [8–10]. In these cases, the subleading non- s -wave pairing channels from EPC should be taken into account.

First-principles analysis along this direction is very limited. The pioneering calculation by Wan and

Savrasov [6] on doped Bi_2Se_3 employed a set of orthogonal polynomials defined on the Fermi surface (FS), known as FS harmonics [11], to project EPC to different pairing channels. The results clearly indicate that non- s -wave pairing information is readily encoded in the standard DFPT EPC data. However, the construction of FS harmonics is tedious, especially for complicated FS's. The functions depend on not only the crystal structure, but also FS geometry, which hinders high-throughput applications of the method.

Nomoto et al. [12] extended DFT for superconductivity (SCDFT) [13, 14] to deal with odd-parity pairing in an *ab initio* way. The treatment is exact when S_z is a good quantum number, e.g. without the spin-orbit coupling (SOC). When SOC is strong, however, the exact forms of odd-parity pairing in the basis of Kohn-Sham (K-S) eigenstates are not known *a priori*.

The primary goal of this Article is to formulate an efficient and simple-to-use algorithm for first-principles EPC pairing-channel analysis. The key is to properly solve gauge indeterminacy of the EPCs. After that, we show that the pairing channels can be resolved by standard matrix diagonalization. We call this approach the “direct diagonalization method” (DDM). In Sec. II, we will first review the general theory of phonon-mediated pairing interactions, and then discuss the gauge complexity. In the end, we present the DDM method. In Sec. III, the DDM method is applied to several realistic material systems. Section IV concludes this Article.

* zliu23@buaa.edu.cn

II. THEORETICAL FRAMEWORK

A. General theory

We start by considering a system with inversion (\mathcal{I}) and time-reversal (\mathcal{T}) symmetries. Without \mathcal{I} , the definition of parity is missing, and the gap function is in general a mixture of odd and even parities. Without \mathcal{T} , the scenario is complicated by the coexistence of magnetism, which we defer for future works. The combination of \mathcal{I} and \mathcal{T} enforces that every eigenstate is at least doubly degenerate. Every K-S eigenstates can then be labeled by a band index n , the lattice momentum \mathbf{k} and a pseudospin variable $s = \pm$.

The DFT+DFPT calculations quantify the following EPC Hamiltonian:

$$H_{ep} = \sum_{n,m,\mathbf{k},\mathbf{q},s,s'} g_{n\mathbf{k}s,m\mathbf{k}+\mathbf{q}s'}^\dagger c_{m\mathbf{k}+\mathbf{q}s'}^\dagger c_{n\mathbf{k}s} (b_{v,\mathbf{q}}^\dagger + b_{v,-\mathbf{q}}),$$

in which $c_{n\mathbf{k}s} (b_{v,\mathbf{q}})$ is the annihilation operator of the electron (phonon) eigenstate. The phonons are labeled by a mode index v and the lattice vector \mathbf{q} . $g_{n\mathbf{k}s,m\mathbf{k}+\mathbf{q}s'}^v$ is the EPC coefficient.

Within the second-order perturbation, the EPC generates the pairing interaction:

$$H_{pair} = - \sum_{n\mathbf{k},m\mathbf{k}',s_1,2,3,4} V_{s_2,s_1;s_3,s_4}(n\mathbf{k},m\mathbf{k}') \quad (1)$$

$$c_{m\mathbf{k}'s_3}^\dagger c_{m,-\mathbf{k}',s_4}^\dagger c_{n,-\mathbf{k},s_2} c_{n\mathbf{k}s_1},$$

with

$$V_{s_2,s_1;s_3,s_4}(n\mathbf{k},m\mathbf{k}') = \sum_v \frac{g_{n\mathbf{k}s_1,m\mathbf{k}'s_3}^v g_{n-\mathbf{k}s_2,m-\mathbf{k}'s_4}^v}{\omega_{\mathbf{k}'-\mathbf{k},v}} \times \delta(\epsilon_{n\mathbf{k}} - \epsilon_F) \delta(\epsilon_{m\mathbf{k}'} - \epsilon_F), \quad (2)$$

in which $\epsilon_{n\mathbf{k}} (\omega_{\mathbf{k}'-\mathbf{k},v})$ is the electron (phonon) eigenenergy, and we restrict the involved electrons residing at the Fermi energy (ϵ_F).

To bridge the interaction to a matrix analysis problem, it is convenient to view $V_{s_2,s_1;s_3,s_4}(n\mathbf{k},m\mathbf{k}')$ as the components of a matrix \mathbb{V} and define a vector operator $\hat{\Delta}$ with its components

$$\hat{\Delta}(n\mathbf{k}s_1s_2) = c_{n,-\mathbf{k},s_2} c_{n\mathbf{k}s_1}, \quad (3)$$

which physically annihilates a Cooper pair consisting of electrons at the $|n\mathbf{k}s_1\rangle$ and $|n,-\mathbf{k},s_2\rangle$ states. Its ground-state expectation value $\langle \hat{\Delta}(n\mathbf{k}s_1s_2) \rangle$ reflects the SC order parameter. Eq. (1) is then transformed into a compact quadratic form:

$$H_{pair} = -\hat{\Delta}^\dagger \mathbb{V} \hat{\Delta}. \quad (4)$$

Roughly, diagonalizing the kernel \mathbb{V} is supposed to decompose different pairing channels.

B. Gauge complexity

The complexity is that EPCs are routinely evaluated on a k -mesh in the full Brillouin zone, where K-S orbitals at each k point is treated independently with ‘‘gauge’’ indeterminacy. It is straightforward to see that $\hat{\Delta}(n\mathbf{k}s_1s_2)$ is gauge dependent by adding an arbitrary U(1) phase to $c_{n\mathbf{k}s_1}$. More critically, the double degeneracy allows any recombination of the degenerate K-S orbitals as the eigenstate. Therefore, an arbitrary SU(2) rotation usually also presents in the first-principles data, especially for strong SOC systems, which hinders a textbook definition of the pairing symmetry assuming s_1, s_2 in $\hat{\Delta}$ refer to a global spin axis. It is worth mentioning that maximally localized Wannier function interpolation is a powerful procedure for *ab initio* gauge fixing [15], but to properly specify the pseudo spin index, especially for strong SOC systems, could still be tricky.

C. DDM solution

The main advantage of the DDM method is to avoid specifying the gauge condition, such that the computational procedure could label the pairing channel in any gauge. Let us denote

$$\mathcal{T} c_{n\mathbf{k}s} \equiv s \tilde{c}_{n,-\mathbf{k},-s}, \quad (5)$$

in which the sign s before \tilde{c} is used to explicitly track the $\mathcal{T}^2 = -1$ condition for an electron. The tilde symbol implies that $(\tilde{c}_{n,-\mathbf{k},+}, \tilde{c}_{n,-\mathbf{k},-})$ is allowed to differ from $(c_{n,-\mathbf{k},+}, c_{n,-\mathbf{k},-})$, i.e. the numerical K-S states at $-\mathbf{k}$ without gauge fixing, by an arbitrary U(1) \times SU(2) transformation. Thus defined $\tilde{c}_{n,-\mathbf{k},-s}$ also relates to $c_{n\mathbf{k},-s}$ via spatial inversion as:

$$\mathcal{I} c_{n\mathbf{k},-s} = e^{i\alpha_{n\mathbf{k}}} \tilde{c}_{n,-\mathbf{k},-s}. \quad (6)$$

Note that theoretical analysis usually implicitly assumes $e^{i\alpha_{n\mathbf{k}}} = 1$, which however does not automatically hold for the numerical K-S states. A U(1) transformation $c_{n\mathbf{k}\pm} \rightarrow e^{i\alpha_{n\mathbf{k}\pm}} c_{n\mathbf{k}\pm}$ will lead to an overall phase shift $\alpha_{n\mathbf{k}} = \alpha_{n\mathbf{k}+} + \alpha_{n\mathbf{k}-}$.

We rewrite Eqs. (1) and (2) into

$$H_{pair} = - \sum_{n\mathbf{k},m\mathbf{k}',s_1,2,3,4} V_{s_2,s_1;s_3,s_4}(n\mathbf{k},m\mathbf{k}') \quad (7)$$

$$c_{m\mathbf{k}'s_3}^\dagger c_{m,-\mathbf{k}',s_4}^\dagger \tilde{c}_{n,-\mathbf{k},s_2} c_{n\mathbf{k}s_1},$$

and

$$V_{s_2,s_1;s_3,s_4}(n\mathbf{k},m\mathbf{k}') = \sum_v s_2 s_4 \frac{g_{n\mathbf{k}s_1,m\mathbf{k}'s_3}^v (g_{n\mathbf{k},-s_2,m\mathbf{k}',-s_4}^v)^*}{\omega_{\mathbf{k}'-\mathbf{k},v}} \times \delta(\epsilon_{n\mathbf{k}} - \epsilon_F) \Theta(\epsilon_{m\mathbf{k}'} - \epsilon_F). \quad (8)$$

The emergence of summand sign s_2s_4 is a direct consequence of $\mathcal{T}^2 = -1$ [c.f. Eq. (5)]. A useful point is that the EPC between $\tilde{c}_{m,-\mathbf{k}',s'}$ and $\tilde{c}_{n,-\mathbf{k},s}$ can be readily obtained from that between $c_{m,\mathbf{k}',-s'}$ and $c_{n,\mathbf{k},-s}$ by applying \mathcal{T} , so the tilde states never need to be explicitly constructed.

Accordingly, Eq. (3) is rewritten as

$$\hat{\Delta}(n\mathbf{k}s_1s_2) = \tilde{c}_{n,-\mathbf{k},s_2}c_{n\mathbf{k}s_1}. \quad (9)$$

This definition greatly facilitates numerical analysis of gap function symmetry, because its transformation under \mathcal{I} is well-defined. Referring to Eq. (6), we have

$$\begin{aligned} \mathcal{I}\hat{\Delta}(n\mathbf{k}\pm\pm) &= -\hat{\Delta}(n\mathbf{k}\pm\pm) \\ \mathcal{I}\hat{\Delta}(n\mathbf{k}\pm\mp) &= -\hat{\Delta}(n\mathbf{k}\mp\pm). \end{aligned} \quad (10)$$

Note that the undertermined U(1) phase $e^{i\alpha_{n\mathbf{k}}}$ cancels.

Now, we can construct one even-parity operator:

$$\hat{\Delta}^S(n\mathbf{k}) = \frac{1}{2}[\hat{\Delta}(n\mathbf{k}+-) - \hat{\Delta}(n\mathbf{k}-+)], \quad (11)$$

and three odd-parity operators

$$\begin{aligned} \hat{\Delta}^{T_0}(n\mathbf{k}) &= \frac{1}{2}[\hat{\Delta}(n\mathbf{k}+-) + \hat{\Delta}(n\mathbf{k}-+)] \\ \hat{\Delta}^{T_{\pm}}(n\mathbf{k}) &= \hat{\Delta}(n\mathbf{k}\pm\pm). \end{aligned} \quad (12)$$

Transforming into this basis, the kernel \mathbb{V} is block diagonalized into the even-parity singlet sector (\mathbb{V}^S) and the odd-parity triplet sector (\mathbb{V}^T). The matrix elements are:

$$\begin{aligned} V^S(n\mathbf{k}, m\mathbf{k}') &= \sum_{vs_1s_3} \frac{|g_{n\mathbf{k}s_1, m\mathbf{k}'s_3}^v|^2}{\omega_{\mathbf{k}'-\mathbf{k},v}} \\ &\times \delta(\epsilon_{n\mathbf{k}} - \epsilon_F)\Theta(\epsilon_{m\mathbf{k}'} - \epsilon_F), \end{aligned} \quad (13)$$

and

$$\begin{aligned} V^T(n\mathbf{k}, m\mathbf{k}') &= \sum_v \left(\begin{array}{cc} g_{n\mathbf{k}+, m\mathbf{k}'+}^v (g_{n\mathbf{k}-, m\mathbf{k}'-}^v)^* & - \sum_s g_{n\mathbf{k}+, m\mathbf{k}'s}^v (g_{n\mathbf{k}-, m\mathbf{k}'s}^v)^* & - g_{n\mathbf{k}+, m\mathbf{k}'-}^v - (g_{n\mathbf{k}-, m\mathbf{k}'+}^v)^* \\ - \sum_s g_{n\mathbf{k}s, m\mathbf{k}'+}^v (g_{n\mathbf{k}s, m\mathbf{k}'-}^v)^* & \sum_{ss'} ss' |g_{n\mathbf{k}s_1, m\mathbf{k}'s_3}^v|^2 & - \sum_s g_{n\mathbf{k}s, m\mathbf{k}'-}^v (g_{n\mathbf{k}s, m\mathbf{k}'+}^v)^* \\ - g_{n\mathbf{k}-, m\mathbf{k}'+}^v (g_{n\mathbf{k}+, m\mathbf{k}'-}^v)^* & - \sum_s g_{n\mathbf{k}-, m\mathbf{k}'s}^v (g_{n\mathbf{k}+, m\mathbf{k}'s}^v)^* & g_{n\mathbf{k}-, m\mathbf{k}'-}^v - (g_{n\mathbf{k}+, m\mathbf{k}'+}^v)^* \end{array} \right) \\ &\times \frac{\delta(\epsilon_{n\mathbf{k}} - \epsilon_F)\Theta(\epsilon_{m\mathbf{k}'} - \epsilon_F)}{\omega_{\mathbf{k}'-\mathbf{k},v}}. \end{aligned} \quad (14)$$

It is heuristic to inspect that the average of $V^S(n\mathbf{k}, m\mathbf{k}')$ normalized by the Fermi surface density of states is the isotropic dimensionless EPC strength λ commonly used to predict the s -wave T_c [1], which implicitly assumes that the matrix components do not contain any singular variation. The weak-SOC approximation employed by Nomoto et al. [12] to evaluate odd-parity pairing can be viewed as neglecting the off-diagonal matrix elements in Eq. (14).

Without introducing these approximations, we proceed by directly diagonalizing $\mathbb{V}^{S(T)}$:

$$\begin{aligned} \mathbb{V}^S|\sigma_i\rangle &= \lambda_i^S|\sigma_i\rangle, \\ \mathbb{V}^T|\tau_i\rangle &= \lambda_i^T|\tau_i\rangle. \end{aligned} \quad (15)$$

In practice, we non-dimensionlize \mathbb{V} by $V_{s_2, s_1; s_3, s_4}(n\mathbf{k}, m\mathbf{k}') \rightarrow V_{s_2, s_1; s_3, s_4}(n\mathbf{k}, m\mathbf{k}')N_{n\mathbf{k}}$, where $N_{n\mathbf{k}}$ is the contribution of the $|n\mathbf{k}s\rangle$ state to the total density of states. This makes the largest λ_i^S , which we denote as λ_{max}^S , directly comparable to the isotropic dimensionless EPC strength λ reported in literature. The largest λ_i^T (λ_{max}^T) gives the leading odd-parity spin-triplet pairing strength.

The eigenvectors:

$$\begin{aligned} |\sigma_i\rangle &= [\xi_i(n_1\mathbf{k}_1), \xi_i(n_1\mathbf{k}_2), \dots]^T, \\ |\tau_i\rangle &= [\xi_i(T_0, n_1\mathbf{k}_1), \xi_i(T_+, n_1\mathbf{k}_1), \xi_i(T_-, n_1\mathbf{k}_1), \dots]^T \end{aligned} \quad (16)$$

reflect the \mathbf{k} -space symmetry of the corresponding pairing channel, which can be classified by the irreducible representations (irreps.) of the symmetry group.

There is still one remaining issue. So far, $\hat{\Delta}(n\mathbf{k}s_1s_2) = \tilde{c}_{n,-\mathbf{k},s_2}c_{n\mathbf{k}s_1}$ and $\hat{\Delta}(n, -\mathbf{k}s_2s_1) = \tilde{c}_{n\mathbf{k}s_1}c_{n,-\mathbf{k},s_2}$ are treated as independent operators, which are actually related by an undecided gauge transformation and the fermion anticommutation relation. (Mathematically, the basis of \mathbb{V} is overcomplete.) Therefore, additional constraints should be applied to the eigenvectors.

Specifically, the symmetrized even-parity operator $\hat{\Delta}^S(n\mathbf{k})$ is U(1) and SU(2) invariant. The constraint to $|\sigma_i\rangle$ is simply $\xi_i(n_m\mathbf{k}_j) = \xi_i(n_m, -\mathbf{k}_j)$. In practice, it means that eigenvectors inconsistent with it should be discarded.

For the odd-parity sector, the eigenvector coefficients $\xi_i(T_0, n_1\mathbf{k}_1)$, $\xi_i(T_+, n_1\mathbf{k}_1)$ and $\xi_i(T_-, n_1\mathbf{k}_1)$ mutually transform under the SU(2) rotation like a spin-1 object. Our recipe is to find a rotation such that $\xi_i(T_+, n_1\mathbf{k}_1)$

and $\xi_i(T_-, n_1 \mathbf{k}_1)$ vanish. Numerically, this is equivalent to diagonalizing a 2×2 matrix: $\xi_i(T_0, n_1 \mathbf{k}_1) \sigma_z + \frac{\xi_i(T_+, n_1 \mathbf{k}_1) + \xi_i(T_-, n_1 \mathbf{k}_1)}{2} \sigma_x + \frac{\xi_i(T_+, n_1 \mathbf{k}_1) - \xi_i(T_-, n_1 \mathbf{k}_1)}{2} \sigma_y$ into $\tilde{\xi}_i(T_0, n_1 \mathbf{k}_1) \sigma_z$. Note that the \mathcal{T} symmetry enforces $\xi_i(T_+, n_1 \mathbf{k}_1) = \xi_i^*(T_-, n_1 \mathbf{k}_1)$, so this matrix is Her-

mitian and $\tilde{\xi}_i(T_0, n_1 \mathbf{k}_1) \sigma_z$ is real. The constraint to $|\tau_i\rangle$ is $\tilde{\xi}_i(n_m \mathbf{k}_j) = -e^{i\Theta_{n_m \mathbf{k}_j}} \xi_i(n_m, -\mathbf{k}_j)$, in which $\Theta_{n_m \mathbf{k}_j}$ is the angle between $\langle n_m \mathbf{k}_j + |\vec{S}| n_m \mathbf{k}_j + \rangle$ and $\langle n_m, -\mathbf{k}_j, + | \vec{S} | n_m, -\mathbf{k}_j, + \rangle$ after the same rotations deciding $\xi_i(T_0, n_m \mathbf{k}_j)$ and $\tilde{\xi}_i(T_0, n_m, -\mathbf{k}_j)$. The \mathcal{T} symmetry enforces $\Theta_{n_m \mathbf{k}_j} = \pm \pi$.

Table I Material-dependent parameters for the DFT and DFPT calculations.

Materials	Energy cutoff (Ha)	QE k -mesh	QE q -mesh	EPW k -mesh	EPW q -mesh
Bi ₂ Se ₃ (slab)	60	30×30×1	4×4×1	180×180×1	180×180×1
Bi ₂ Se ₃	40	12×12×12	3×3×3	20×20×20	20×20×20
SnTe	60	12×12×12	6×6×6	20×20×20	20×20×20
Bi ₂ Pd	60	12×12×12	4×4×4	20×20×20	20×20×20
Al	80	10×10×10	10×10×10	30×30×30	30×30×30
Pd	60	12×12×12	6×6×6	20×20×20	20×20×20
Cd	60	12×12×12	6×6×6	20×20×20	20×20×20
Ta	60	10×10×10	10×10×10	20×20×20	20×20×20
Pb	60	12×12×12	6×6×6	20×20×20	20×20×20
Hg	70	18×18×18	3×3×3	18×18×18	18×18×18

III. APPLICATIONS

Below we apply DDM to several representative materials. The input data to construct \mathbb{V} are obtained from Quantum Espresso with GGA-PBE exchange correlation functional [16–18], optimized norm-conserving Vanderbilt pseudopotential [19, 20] and a 0.01 Ry Methfessel-Paxton smearing [21] for all materials. The convergence criteria are $10^{-8}(a, u)$ for lattice and atomic relaxations, and $10^{-12}(a, u)$ for electronic iterations. The EPCs from Quantum Espresso are further Wannier interpolated by using the EPW code [22]. Material-dependent setups are summarized in Tab. I. Our DDM code to analyze \mathbb{V} is accessible at: [https://github.com/ZimengZengTHU/Resolving-different-superconducting-pairing].

A. Bi₂Se₃ slab

We first consider an intuitively transparent example - the well-known 3D topological insulator Bi₂Se₃ [23]. By cleaving a slab [Fig. 1(a)], helical bands form on both surfaces [Fig. 1(b)]. Within the bulk gap, the helical surface states lead to a doubly-degenerate FS. Since the other bulk bands are fully gaped, the band index n can be omitted. According to our definitions [Eqs. (5) and (9)], $\hat{\Delta}(\mathbf{k} \pm \mp)$ refers to intra-surface pairing, and $\hat{\Delta}(\mathbf{k} \pm \pm)$

refers to inter-surface pairing.

When the slab is infinitely thick, the two surfaces are decoupled. Therefore, $\langle \hat{\Delta}(\mathbf{k} \pm \pm) \rangle = 0$, and there is no constraint on the relative phase of $\langle \hat{\Delta}(\mathbf{k} + -) \rangle$ and $\langle \hat{\Delta}(\mathbf{k} - +) \rangle$, indicating degeneracy between the leading $\langle \hat{\Delta}^S \rangle$ and $\langle \hat{\Delta}^{T_0} \rangle$. For a finite thick slab, Cooper pairs related by spin-conserving inter-surface scatterings, e.g. $\tilde{c}_{-\mathbf{k},+} c_{\mathbf{k},-} \rightarrow \tilde{c}_{\mathbf{k},+} c_{-\mathbf{k},-}$, tend to establish a unified phase to take advantage of the attraction, making Δ^S the dominating pairing channel. This argument suggests that the spatial separation of the surface states makes the the leading pairing channels from the odd-parity and even-parity sectors close in strength.

Figure 1(c) plots the DDM-predicted largest eigenvalues $\lambda_{max}^{S(T)}$ of $\mathbb{V}^{S(T)}$ in a two-quintuple layer Bi₂Se₃ slab as a function of the Fermi level. In terms of the irreducible representations of the slab point group (D_{3d}), the associated eigenstates are assigned to A_{1g} and A_{1u} , respectively. The ratio $\lambda_{max}^T / \lambda_{max}^S$ reaches up to 76.3%, which pedagogically shows the relevance of EPC calculations for a complete understanding of non- s -wave superconductivity.

We note that pairing requires nonvanishing density of states, so in our calculation the Fermi level is purposely elevated away from the Dirac point [Fig. 1(b)]. The range of Fermi level for EPC calculations as shadowed in Fig. 1(b) corresponds to doping 0.043~0.052 electrons

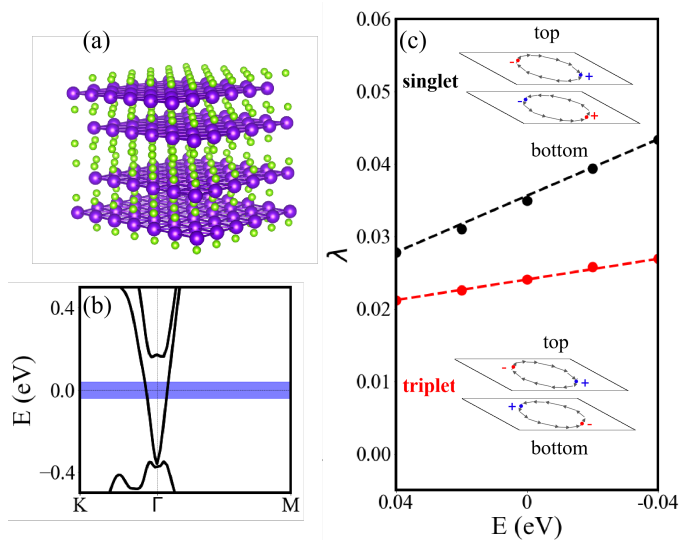


FIG. 1. (a) Atomic structure of a two-quintuple layer Bi_2Se_3 slab employed for the DFT+DFPT calculation; (b) Electron band structure; the shadowed region indicates the range of the electron-doped Fermi level for the EPC and DDM calculations; (c) Leading pairing strength in the spin-singlet and spin-triplet sectors; the insets schematically decompose the Fermi surfaces into two circles localized on the two surfaces of the slabs. The symmetry of the corresponding DDM eigenvector [c.f. Eq. (16)] is reflected by plotting the signs of its components at a selected pair of $\pm\mathbf{k}$ points.

per unit cell, which however is still not enough to support significantly large intrinsic λ 's. Experimentally, proximity to a bulk superconductor is typically required to achieve surface SC [24].

B. Doped Bi_2Se_3 and SnTe

The possible topological SC in $\text{Cu}_x\text{Bi}_2\text{Se}_3$ [25, 26] and $\text{Sn}_{1-x}\text{In}_x\text{Te}$ [27] has motivated several previous EPC calculations on bulk Bi_2Se_3 and SnTe with charge doping [6, 12, 28]. Using DDM, we can obtain a systematic differentiation of pairing channels (Figs. 2 and 3). We choose to add 0.12 (0.1) electrons per unit cell to Bi_2Se_3 (SnTe) in line with the previous calculations to make quantitative comparisons.

For doped Bi_2Se_3 , the leading even-parity pairing $\lambda_{A_{1g}}$ is calculated to be 0.315, in good agreement with the isotropic λ reported in [28]. The leading odd-parity pairing λ_{E_u} is one order of magnitude smaller than $\lambda_{A_{1g}}$, in agreement with Namoto et al.'s qualitative conclusion based on the weak-SOC approximation [12]. We should mention that Wan and Savarasov [6] in contrast predicted large odd-parity pairings $\lambda_{A_{2u}}$ and λ_{E_u} based on the FS harmonics projection. This prediction was ra-

Irrep	Strength	Eigenvector
A_{1g}	0.315	
$E_u(1)$	0.046	
$E_u(2)$	0.045	
$E_u(3)$	0.043	
$E_u(4)$	0.0047	
A_{2u}	0.041	

FIG. 2. DDM analysis results of electron-doped Bi_2Se_3 . The eigenvalues (λ_i) and eigenvectors are classified by the irreps. of the D_{3d} point group. The color contour shows the sign and magnitude of the eigenvector components on the Fermi surface.

tionalized by a singular EPC associated with the acoustic phonon at $q=(0,0,0.04)$ (in terms of the reciprocal vectors). However, this singular EPC was not reproduced in either [28] or [12]. We note that our phonon linewidth calculation gives very similar results to those reported in [28] and [12]. In particular, no singularity is observed at $q=(0,0,0.04)$.

With respect to doped SnTe , DDM predicts that there is no odd-parity pairing channel of the same order of magnitude in strength as the leading even-parity pairing channel. The ratio between λ_{A_{1u}/E_u} and $\lambda_{A_{1g}}$ is roughly around 0.1, in agreement with [12]. The leading odd-parity gap function shown in [12] can also be nicely compared with our $E_u(1)$ eigenstate as plotted in Fig. 3. The other odd-pairing eigenstates of comparative strength have not been shown before.

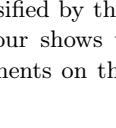
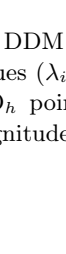
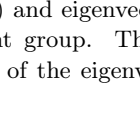
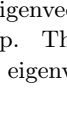
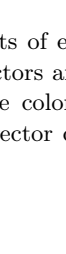
Irrep	Strength	Eigenvector
A_{1g}	0.365	
$E_u(1)$	0.0508	
A_{1u}	0.0494	
$A_{1u}(2)$	0.0481	
$E_u(3)$	0.0439	

FIG. 3. DDM analysis results of electron-doped SeTe. The eigenvalues (λ_i) and eigenvectors are classified by the irreps. of the O_h point group. The color contour shows the sign and magnitude of the eigenvector components on the Fermi surface.

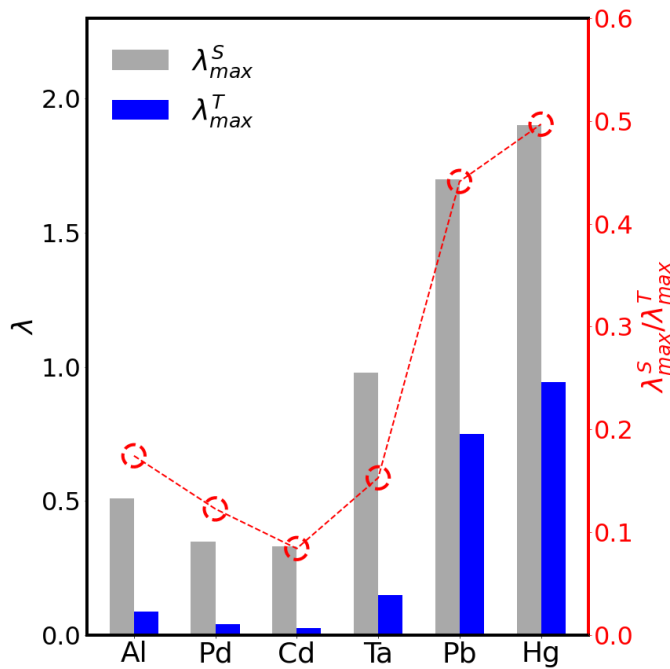


FIG. 4. leading even-parity(black),leading odd-parity(blue),sub-leading even-parity(red) superconducting pairing channels are calculated by our method

C. Elemental metals

Figure 4 summarizes $\lambda_{max}^{S(T)}$ of superconducting elemental metals, including Pb,Ta,Al,Pd,Hg,Cd. For all these

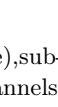
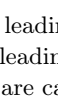
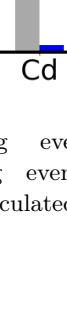
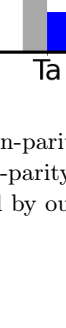
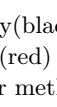
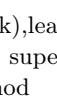
Irrep	Strength	Eigenvector
A_{1g}	1.7	
A_{1u}	0.75	
T_{2u}	0.47	
T_{2g}	0.2	
E_{2u}	0.18	
E_g	0.17	

FIG. 5. DDM analysis results of Pb. The eigenvalues (λ_i) and eigenvectors are classified by the irreps. of the O_h point group. The color contour shows the sign and magnitude of the eigenvector components on the Fermi surface.

materials, λ_{max}^S obtained from the DDM method can be well compared with the isotropic dimensionless λ reported in literature [29–31]. The ratio $\lambda_{max}^T/\lambda_{max}^S$ varies between 0.1 and 0.5. It is interesting to note that the highest ratio occurs in Pb and Hg, in which EPC is known to be quite large. In experiment, Pb is a frequently used component to search for topological superconductivity [32–35]. In Fig. 5, we plot the leading pairing channels of Pb resolved by DDM. It is worth further investigations to identify the key factors for a high $\lambda_{max}^T/\lambda_{max}^S$ ratio.

IV. CONCLUSION

In summary, we present an efficient and simple-to-use algorithm for first-principles EPC pairing-channel analysis. It is theoretically known that the leading pairing channel by EPC is s -wave [7]. All our first-principles results support this perception. Meanwhile, the calculations also indicate that EPC contains non-negligible non- s -wave channels. These quantifications and further applications in a high-throughput manner are expected to provide useful guide to realize exotic superconductivity.

-
- [1] F. Giustino, Electron-phonon interactions from first principles, *Rev. Mod. Phys.* **89**, 015003 (2017).
- [2] S. Baroni, S. de Gironcoli, A. Dal Corso, and P. Giannozzi, Phonons and related crystal properties from density-functional perturbation theory, *Rev. Mod. Phys.* **73**, 515 (2001).
- [3] W. McMillan, Transition temperature of strong-coupled superconductors, *Physical Review* **167**, 331 (1968).
- [4] G. Eliashberg, Interactions between electrons and lattice vibrations in a superconductor, *Sov. Phys. JETP* **11**, 696 (1960).
- [5] L. Fu and E. Berg, Odd-parity topological superconductors: theory and application to $\text{Cu}_x\text{Bi}_2\text{Se}_3$, *Physical review letters* **105**, 097001 (2010).
- [6] X. Wan and S. Y. Savrasov, Turning a band insulator into an exotic superconductor, *NATURE COMMUNICATIONS* **5**, 10.1038/ncomms5144 (2014).
- [7] P. Brydon, S. Das Sarma, H.-Y. Hui, and J. D. Sau, Odd-parity superconductivity from phonon-mediated pairing: Application to $\text{Cu}_x\text{Bi}_2\text{Se}_3$, *Physical Review B* **90**, 184512 (2014).
- [8] F. Schrodi, P. M. Oppeneer, and A. Aperis, Unconventional superconductivity mediated solely by isotropic electron-phonon interaction, *Physical Review B* **104**, L140506 (2021).
- [9] A. Aperis, P. Kotetes, G. Varelogiannis, and P. M. Oppeneer, Small- q phonon-mediated unconventional superconductivity in the iron pnictides, *Phys. Rev. B* **83**, 092505 (2011).
- [10] Z.-X. Shen, A. Lanzara, S. Ishihara, and N. Nagaosa, Role of the electron-phonon interaction in the strongly correlated cuprate superconductors, *Philosophical magazine B* **82**, 1349 (2002).
- [11] P. B. Allen, Fermi-surface harmonics: A general method for nonspherical problems. application to boltzmann and eliasberg equations, *Phys. Rev. B* **13**, 1416 (1976).
- [12] T. Nomoto, M. Kawamura, T. Koretsune, R. Arita, T. Machida, T. Hanaguri, M. Kriener, Y. Taguchi, and Y. Tokura, Microscopic characterization of the superconducting gap function in $\text{Sn}_{1-x}\text{In}_x\text{Te}$, *Phys. Rev. B* **101**, 014505 (2020).
- [13] M. Lüders, M. A. L. Marques, N. N. Lathiotakis, A. Floris, G. Profeta, L. Fast, A. Continenza, S. Massidda, and E. K. U. Gross, Ab initio theory of superconductivity. i. density functional formalism and approximate functionals, *Phys. Rev. B* **72**, 024545 (2005).
- [14] M. A. L. Marques, M. Lüders, N. N. Lathiotakis, G. Profeta, A. Floris, L. Fast, A. Continenza, E. K. U. Gross, and S. Massidda, Ab initio theory of superconductivity. ii. application to elemental metals, *Phys. Rev. B* **72**, 024546 (2005).
- [15] N. Marzari, A. A. Mostofi, J. R. Yates, I. Souza, and D. Vanderbilt, Maximally localized wannier functions: Theory and applications, *Rev. Mod. Phys.* **84**, 1419 (2012).
- [16] P. Giannozzi, O. Andreussi, T. Brumme, O. Bunau, M. B. Nardelli, M. Calandra, R. Car, C. Cavazzoni, D. Ceresoli, M. Cococcioni, *et al.*, Advanced capabilities for materials modelling with Quantum ESPRESSO, *Journal of physics: Condensed matter* **29**, 465901 (2017).
- [17] P. Giannozzi, S. Baroni, N. Bonini, M. Calandra, R. Car, C. Cavazzoni, D. Ceresoli, G. L. Chiarotti, M. Cococcioni, I. Dabo, *et al.*, Quantum espresso: a modular and open-source software project for quantum simulations of materials, *Journal of physics: Condensed matter* **21**, 395502 (2009).
- [18] J. P. Perdew, K. Burke, and M. Ernzerhof, Perdew, burke, and ernzerhof reply, *Physical Review Letters* **80**, 891 (1998).
- [19] D. R. Hamann, Optimized norm-conserving vanderbilt pseudopotentials, *Phys. Rev. B* **88**, 085117 (2013).
- [20] D. R. Hamann, Erratum: Optimized norm-conserving vanderbilt pseudopotentials [phys. rev. b 88, 085117 (2013)], *Phys. Rev. B* **95**, 239906 (2017).
- [21] M. Methfessel and A. T. Paxton, High-precision sampling for brillouin-zone integration in metals, *Phys. Rev. B* **40**, 3616 (1989).
- [22] S. Poncé, E. R. Margine, C. Verdi, and F. Giustino, Epw: Electron-phonon coupling, transport and superconducting properties using maximally localized wannier functions, *Computer Physics Communications* **209**, 116 (2016).
- [23] X.-L. Qi and S.-C. Zhang, Topological insulators and superconductors, *Rev. Mod. Phys.* **83**, 1057 (2011).
- [24] M.-X. Wang, C. Liu, J.-P. Xu, F. Yang, L. Miao, M.-Y. Yao, C. Gao, C. Shen, X. Ma, X. Chen, *et al.*, The coexistence of superconductivity and topological order in the bi_2se_3 thin films, *Science* **336**, 52 (2012).
- [25] Y. S. Hor, A. J. Williams, J. G. Checkelsky, P. Roushan, J. Seo, Q. Xu, H. W. Zandbergen, A. Yazdani, . f. N. Ong, and R. J. Cava, Superconductivity in $\text{Cu}_x\text{Bi}_2\text{Se}_3$ and its implications for pairing in the undoped topological insulator, *Physical review letters* **104**, 057001 (2010).
- [26] S. Sasaki, M. Kriener, K. Segawa, K. Yada, Y. Tanaka, M. Sato, and Y. Ando, Topological superconductivity in $\text{cu}_x\text{bi}_2\text{se}_3$, *Phys. Rev. Lett.* **107**, 217001 (2011).
- [27] S. Sasaki, Z. Ren, A. Taskin, K. Segawa, L. Fu, and Y. Ando, Odd-parity pairing and topological superconductivity in a strongly spin-orbit coupled semiconductor, *Physical review letters* **109**, 217004 (2012).
- [28] X.-L. Zhang and W.-M. Liu, Electron-phonon coupling and its implication for the superconducting topological insulators, *Scientific Reports* **5**, 8964 (2015).
- [29] C. Tresca, G. Profeta, G. Marini, G. B. Bachelet, A. Sanna, M. Calandra, and L. Boeri, Why mercury is a superconductor, *Phys. Rev. B* **106**, L180501 (2022).
- [30] S. Y. Savrasov and D. Y. Savrasov, Electron-phonon interactions and related physical properties of metals from linear-response theory, *Phys. Rev. B* **54**, 16487 (1996).

- [31] P. B. Allen and M. L. Cohen, Pseudopotential calculation of the mass enhancement and superconducting transition temperature of simple metals, *Phys. Rev.* **187**, 525 (1969).
- [32] K. Xie, P. Li, L. Liu, R. Zhang, Y. Xia, H. Shi, D. Cai, Y. Gu, L. She, Y. Song, *et al.*, Tuning superconductivity in highly crystalline $Pb_{1-x}Bi_x$ alloy ultrathin films at atomic level, *Physical Review B* **107**, 104511 (2023).
- [33] I. Pletikosić, T. Yilmaz, B. Sinkovic, A. P. Weber, G. D. Gu, and T. Valla, Possible topological superconductivity in the topological crystalline insulator $(Pb_{1-x}Sn_x)_{1-y}In_yTe$, *Physical Review B* **108**, 205157 (2023).
- [34] S.-Y. Guan, P.-J. Chen, M.-W. Chu, R. Sankar, F. Chou, H.-T. Jeng, C.-S. Chang, and T.-M. Chuang, Superconducting topological surface states in the noncentrosymmetric bulk superconductor $PbTaSe_2$, *Science advances* **2**, e1600894 (2016).
- [35] T. Cren, Two-dimensional topological superconductivity in $Pb/Co/Si(111)$, *SUPERSTRIPES*, 263 (2017).